Journal of Siberian Federal University. Engineering & Technologies, 2018, 11(4), 409-418
~ ~ ~

УДК 669.715

The Impact of Recycling on the Mechanical Properties of 6XXX Series Aluminum Alloys

Samuel R. Wagstaff*
Novelis Inc.
2 route des Laminoirs, CH-3960 Sierre, Switzerland

Received 26.01.2018, received in revised form 29.04.2018, accepted 18.05.2018

Increasing the recycle content of a production stream is one of the easiest methods to reduce the cost of wrought aluminum products. This has economic and environmental benefits, but closed loop recycling systems do not reflect the conservation of the original composition, due to so called "tramp elements". To understand the influence of certain tramp elements, a campaign of 950 AA6008 ingots were cast reflecting the entire scope of the composition window for this alloy, and the mechanical properties subsequently analyzed.

Keywords: recycling, tramp elements, mechanical properties.

Citation: Wagstaff S.R. The impact of recycling on the mechanical properties of 6XXX series aluminum alloys, J. Sib. Fed. Univ. Eng. technol., 2018, 11(4), 409-418. DOI: 10.17516/1999-494X-0063.

Влияние рециклинга на механические свойства алюминиевых сплавов серии 6XXX

Самуэль Р. Вагстафф
Novelis Inc.
Швейцария, CH-3960 Sierre, route des Laminoirs, 2

Повышение доли содержания вторичного металла в производственной цепочке является одним из самых простых способов снижения стоимости продукции из деформируемых алюминиевых сплавов. Это имеет экономические и экологические преимущества, но системы рециклинга замкнутого контура не отражают сохранение исходного состава из-за так называемых остаточных элементов. Чтобы понять влияние конкретных остаточных элементов, было произведено 950 слитков из сплава AA6008, отразивших весь диапазон состава этого сплава, и затем проанализированы механические свойства.

Ключевые слова: рециклинг, остаточные элементы, механические свойства.

* Corresponding author E-mail address: Samuel.Wagstaff@novelis.adityabirla.com

Introduction

Recycling is both economically and environmentally beneficial of recycling. Aluminum has one of the largest energy incentives when comparing primary and secondary production: 186 MJ/kg for primary compared to 10-20 MJ/kg for secondary when compared to other materials with high worldwide production volumes [1]. Many aluminum producers have fixed targets for the use of secondary stream materials due to financial, energy, and environmental savings goals imposed by government or management. Although these fixed targets are useful, but there is rarely a 100 % compositional return on recycled products. Impurities accumulate during use and processing which makes the achievement of these goals increasingly more difficult [2].

Due to the benefit of financial, energy, and environmental savings, the search for increased recycle content continues. This has also led to an increasing number of scientific studies that indicate that the accumulation of so-called “tramp elements” is a growing problem and concern. In aluminum processing, there is a significant list of problematic elements, which can affect mechanical or chemical properties of alloys. These elements include Si, Mg, Ni, Pb, Cr, Fe, Cu, V, and Mn [3-9].

The incorporation of secondary metals is a metallurgical decision, which is fundamentally governed by the laws of thermodynamics, where the separation of unwanted elements has a given cost of removal. Without an economical or evident methodology to remove these undesired tramp elements, melt practitioners must keep in mind customer needs and desires when incorporating them into the production stream.

Background

Iron influences the performance of wrought products following thermo-mechanical processing so it is of particular interest to the aluminum industry. Iron is nearly uniformly found along grain boundaries forming complex intermetallic networks which have some benefits in subsequent downstream processes (recrystallization for example). By tightly controlling the compositional windows, desired iron compound is generally formed. As the limits of these windows are approached due to increased secondary material, the precise volume fraction and even species of these compounds can change (see Appendix 1).

Iron is a common impurity that arises during the production of primary aluminum. Iron is produced via the Bayer Process, which then converts bauxite (naturally occurring ore) into alumina (feedstock). After the subsequent Hall-Héroult electrolytic reduction process takes plave the alumina is converted into molten aluminum (>950 °C). One must also take into account the variations of the ore quality and process parameters. Molten primary aluminum typically contains between 0.02-0.15 % iron, yet the average is around 0.07-0.10 %.

Despite continuous research, there is no currently known methodology of economically removing iron from aluminum. Thus, baseline iron levels are typically the starting point and all further melt activities only serve to increase the iron level. Iron can enter the melt during subsequent downstream processing through two primary mechanisms:

- Liquid aluminum is capable of dissolving iron from unprotected tools and/or furnace equipment. Under equilibrium conditions, iron levels can reach 2.5 wt% in the liquid phase at typical processing temperatures (~700 °C) and up to 5.0 wt% for melts held at 800 °C [10].

- Iron can potentially enter aluminum melts via the addition of low purity alloying materials, e.g. silicon, or via the addition of scrap, that contains higher base levels of iron than primary metal.

Iron levels in aluminum alloys continue to increase with each re-melt cycle, and secondary alloys (recycle based), potentially have much higher iron levels than initial primary based material due to the combinations of these two mechanisms. Typical iron levels in commercial alloys are generally moderate, striking the commercial balance between the benefits of reduced metal cost and the acceptable loss of some mechanical properties.

Although iron can be considered soluble in liquid aluminum and its various alloys, it has extremely low solubility in the solid (maximum 0.05 wt%, 0.025 atm%) [10] and thus it tends to precipitate out with other elements to form intermetallic compounds of various types [11]. In the absence of Si, the dominant phases that form are Al3Fe and Al6Fe, but in the presence of silicon, as is the case in most commercial alloys, the dominant phases are hexagonal α-Al8Fe2Si phase and the monoclinic/orthorhombic β-Al5FeSi [12]. If magnesium is present with silicon, an alternative phase can also form π-Al8FeMg3Si6. More detailed information on iron-bearing intermetallic phases can be found in several experimental studies and review papers published over the years [13-18].

The impact of iron on the mechanical properties of aluminum-silicon alloys has been extensively reviewed by several authors [15, 16, 18]. The detrimental effect of iron begins generally at low primary iron levels, but becomes more serious once a critical iron level (dependent on alloy composition) is exceeded. The critical iron level is directly related to the silicon concentration of the alloy. As the silicon content of the alloy increases, the amount of iron that can be tolerated before the β-phase starts to form also increases.

While these conclusions have been justified for a range of foundry alloys, very little work has been done on similar wrought alloys. Given the potential modification of iron intermetallic compounds by magnesium and silicon the present research has been launched on a campaign of 6XXX (Al-Mg-Si) ingots in an attempt to understand the potential influence of iron content on the in-service mechanical properties of this family of alloys.

Experimental procedure

These experiments were collected from a campaign of 950 industrial ingots produced using the DC process. Given the availability of ingots and processing time, AA6008 was chosen as a suitable example alloy. The chemical composition limits for AA6008 are reproduced below in Table 1.

The charges were prepared using a variety of compositions all within the processing window of the desired alloy. The molten alloys were degassed with a rotary degasser bubbling argon, filtered, and grain refined all according to industrial practice. While precise control of each parameter could not be

Table 1. AA6008 composition specification used to prepare melt charges

Si (%)	Mg (%)	Fe (%)	Mn (%)	Cu (%)	Cr (%)
0.5-0.9	0.4-0.7	0.35 Max	0.3 Max	0.30 Max	0.30 Max

ensured through the entirely of 950 ingots, subsequent statistical analysis illustrated that the variations in these practices were irrelevant to the current investigation.

Following casting, the ingots were trimmed, homogenized, and scalped. Afterward the ingots were preheated and hot-rolled on a reversing mill where the processing parameters were controlled to be identical for each of the trial ingots. The ingots were then cold rolled to a final gauge and passed on a Continuous Annealing Solution Heat Treatment (CASH) line to bring them into their final temper. Following CASH treatment, samples were taken from each coil and analyzed for their relevant mechanical properties. Definitions of the mechanical properties can be found in Appendix 2.

Results

Fig. 1 is a contour plot of the Yield Strength (Rp0.2) as a function of both iron and silicon composition. We can see that the yield strength varies through approximately 30 MPa, with lower yield strength values in the lower right-hand corner, corresponding to the region of high iron and low silicon content. The highest yield strengths are found in the upper left-hand corner, corresponding to regions of low iron and high silicon content.

Fig. 2 is a contour plot of the Ultimate Tensile Strength (Rm) as a function of both iron and silicon composition. Similarly to Fig. 1, we can see that the Rm varies through approximately 30 Mpa, with lower Rm values in the lower right-hand corner, corresponding to the region of high iron and

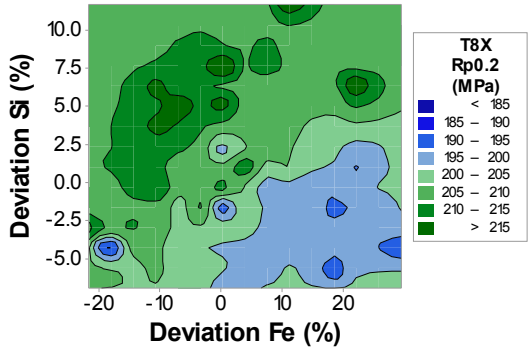

Fig. 1. Contour plot of the T8X Yield Strength (Rp0.2) as a function of Iron and Silicon content

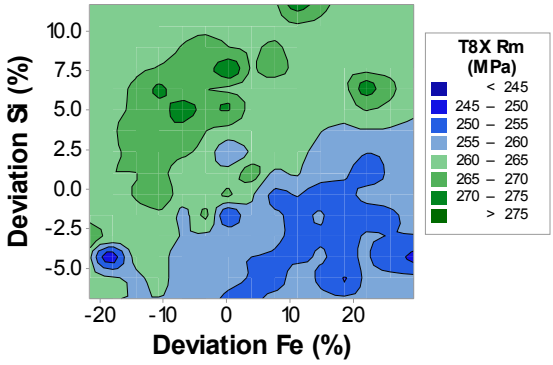

Fig. 2. Contour plot of the T8X Ultimate Tensile Strength (Rm) as a function of Iron and Silicon content

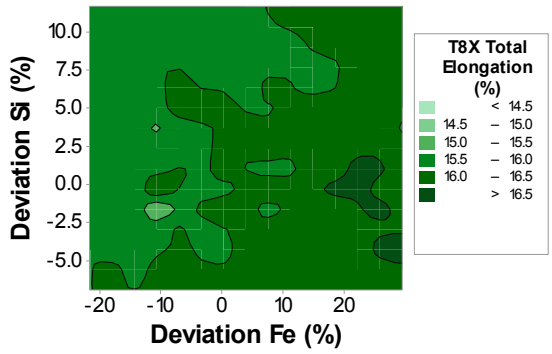

Fig. 3. Contour plot of the T8X Total Elongation as a function of Iron and Silicon content

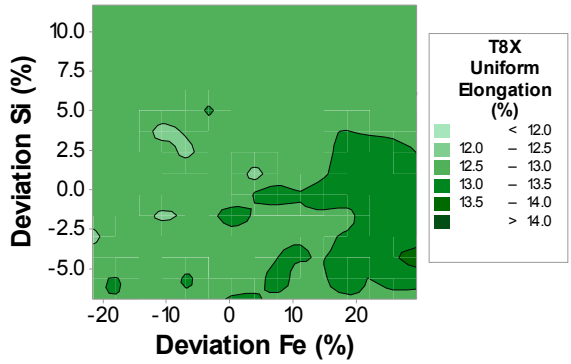

Fig. 4. Contour plot of the T8X Uniform Elongation as a function of Iron and Silicon content

low silicon content. The highest ultimate tensile strengths are found in the upper left-hand corner, corresponding to regions of low iron and high silicon content.

Fig. 3 is a contour plot of the Total Elongation as a function of both iron and silicon composition. We can see that the total elongation varies through approximately 2.0 %, with lower elongation values roughly corresponding to the upper left-hand corner corresponding to higher silicon, and lower iron concentrations.

Fig. 4 is a contour plot of the Uniform Elongation as a function of both iron and silicon composition. Similar to the total elongation, uniform elongation varies through approximately 2.0 %. The map of uniform elongation is fairly constant in the range of 12.5-13.0 %. However, there is a region of higher elongation in the lower right-hand corner corresponding to a region of higher iron and lower silicon.

Discussion

The primary motivation of this study was to examine the effects of increasing recycle content on AA6008 ingots. The nearly 30 MPa swing in tensile properties as a function of iron and silicon content was an unexpected result. From Fig. 1 and 2, the lowest strengths corresponded to regions of high iron and low silicon. The low strength is likely due to the binding of silicon (and magnesium) to iron containing phases during either solidification or the decomposition of the solid solution. Silicon is requisite for the formation of the strengthening Mg_2Si phase will be unavailable following quenching

for precipitation strengthening, thus causing the decrease in strengths (Rp0.2 and Rm). Similar to the results of other authors for Al-Si alloys [15, 16, 18] regarding a critical silicon content (see Background), we can see there exists a line of demarcation between higher and lower strengths, extending from the bottom left (low iron and silicon), upwards and to the right (rising silicon and iron levels). From phase diagram calculations we can ascertain that iron phases can bind up to 50 % of their weight percent of silicon (0.2 % Fe binds 0.1 % Si), which roughly corresponds to the slope of the demarcation line in Fig. 1 and 2. Importantly, high iron contents are not 100 % detrimental to strength values as long as there is excess silicon to replace that bound by the iron phases.

Typically, the introduction of iron into aluminum alloys is associated with a corresponding decrease in elongation and even pre-mature failure due to cracking around the excess iron phases. In the course of this study, such observations were limited as the upper limit of iron had been previously limited to avoid such a scenario. Perhaps counterintuitively, regions with high iron and low silicon tended to have higher elongation than those low iron and high silicon. This is likely due to the decrease in hardening phases (Mg_2Si) in compositions with high iron. The lack of hardening phases corresponds to a reduction in precipitate-dislocation interactions, which leads to a higher elongation, but also a lower strength.

Conclusion

We have performed a set of experiments investigating the impact of increased recycle content on the mechanical properties of an AA6008 wrought aluminum alloy. Increasing iron content without increasing silicon content can reduce mechanical properties by 15MP. Maintaining high silicon content with low iron content can increase mechanical properties by up to 15 MPa, all within the composition limits of AA6008. While these swings may be drastic, it is well known that slight changes in composition can lead to dramatic changes in mechanical properties for aluminum alloys. Composition windows should not be treated as blind processing map, but thermodynamic reactions occurring through the entire process stream must be considered. In the case of AA6008, increased recycle content (increased iron) must be compensated by an increase in silicon in order to balance the iron-silicon reaction. This type of forethought is the only strategy which can be employed when attempting to increase secondary material in wrought alloys.

This article is based on the paper presented at the IX International Congress "Non-ferrous metals and minerals-2017".

APPENDIX 1: Thermodynamics of competitive nucleation

The driving force for the onset of precipitation (D^{α}) of a phase (α) from a liquid with composition X_0^L is schematically represented below in Fig. 5.

From this figure, D^{α} can be written as:

$$D^{\alpha} = G^L(X_0^L) + \left(\frac{\partial G^L}{\partial X^L}\right)_{X_0^L}(X^{\alpha} - X_0^L) - G^{\alpha}. \quad (1)$$

This equation can also be rewritten the following way:

$$D^{\alpha} = G^L(X_0^L) + \left(\frac{\partial G^L}{\partial X^L}\right)_{X_0^L}(X^{\alpha} - X_0^L) - G^L(X_{eq}^L) - \left(\frac{\partial G^L}{\partial X^L}\right)_{X_{eq}^L}(X^{\alpha} - X_{eq}^L). \quad (2)$$

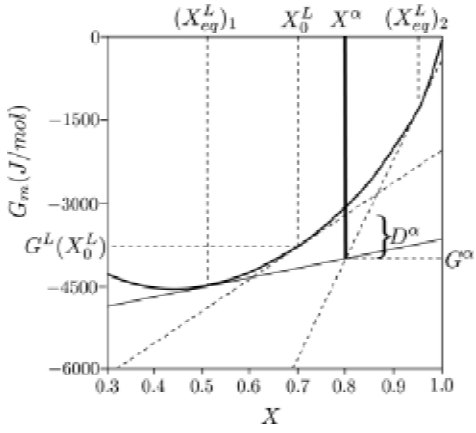

Fig. 5. Illustration of the driving force of precipitation of a binary phase α from a supersaturated liquid solution

If we expand $\left(\frac{\partial G^L}{\partial X^L}\right)_{X_0^L}$ and $G^L(X_{eq}^L)$ using a truncated Taylor's series, this equation then becomes:

$$D^\alpha = (X^\alpha - X_0^L)\, x\, \left(\frac{\partial^2 G^L}{(\partial X^L)^2}\right)_{X_0^L} x\, (X_0^L - X_{eq}^L). \tag{3}$$

As we can see, at low supersaturations, the driving force D^α linearly depends on the supersaturation $X_0^L - X_{eq}^L$, the difference between the initial composition of the liquid and stoichiometric phase $X^\alpha - X_{eq}^L$, and on the curvature of the concentration dependence of the molar Gibb's free energy of the liquid phase $\left(\frac{\partial^2 G^L}{(\partial X^L)^2}\right)_{X_0^L}$.

If we generalize these results to a system of K components, we get:

$$D^\alpha = \left(X_2^\alpha - X_{2,eq}^L, \ldots., X_K^\alpha - X_{K,eq}^L\right) x\, \boldsymbol{H}\, x \begin{bmatrix} X_{2,0}^\alpha - X_{2,eq}^L \\ \vdots \\ X_K^\alpha - X_{K,eq}^L \end{bmatrix}, \tag{4}$$

where $\boldsymbol{H}$ is the Hessian of the molar Gibbs energy.

Recalling that the precipitation of a phase is only possible where $D^\alpha > 0$, there are some concentration regions where this condition is satisfied, and can be defined. We call these regions "nucleability regions" or "nucleability fields", and they cannot span over the entire concentration field. Fig. 6 is a representation of the nucleability region for our precipitated phase (α).

In the nucleability regions of (α) between $(X_{eq}^L)_1$ and $(X_{eq}^L)_2$, the driving forces for precipitation are positive and (α) can be nucleated.

In the case now where two stoichiometric phases have the chance to precipitate from the melt (Fig. 7), the following equation can be written:

$$\begin{gathered} D^{\beta\alpha} = D^\beta - D^\alpha = \\ = \left[G^L(X_0^L) + \left(\frac{\partial G^L}{\partial X^L}\right)_{X_0^L}(X^\beta - X_0^L) - G^\beta\right] - \left[G^L(X_0^L) + \left(\frac{\partial G^L}{\partial X^L}\right)_{X_0^L}(X^\alpha - X_0^L) - G^\alpha\right] = \\ = \left(\frac{\partial G^L}{\partial X^L}\right)_{X_0^L}(X^\beta - X^\alpha) - (G^\beta - G^\alpha). \end{gathered} \tag{5}$$

Fig. 8 shows the variation of driving forces for precipitation of (α) and (β) by changing the composition. It is worthy of note how the initial melt composition affects the driving forces for precipitation

of these phases. It can be seen that by increasing the supersaturation of the melt, the likelihood of the formation of (β) is increased.

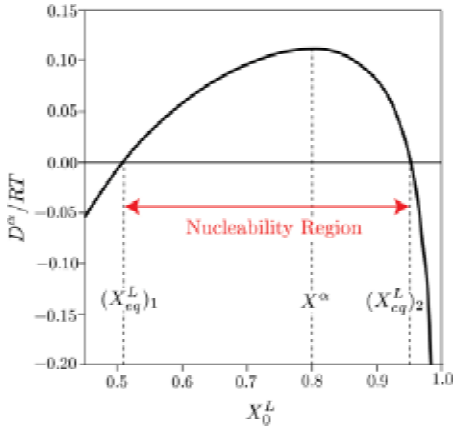

Fig. 6. An example of how the driving force of precipitation depends on the initial melt composition

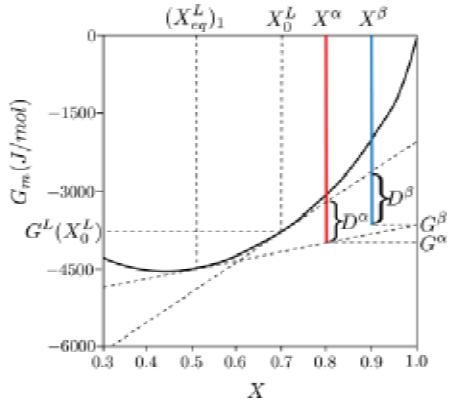

Fig. 7. Driving forces for the onset of precipitation of two competing phases

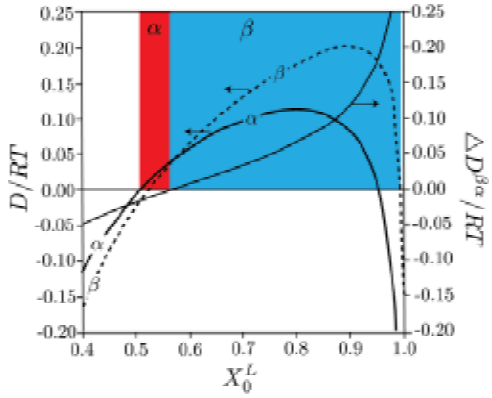

Fig. 8. Illustration of how phase formation depends on the initial composition of the melt

APPENDIX 2

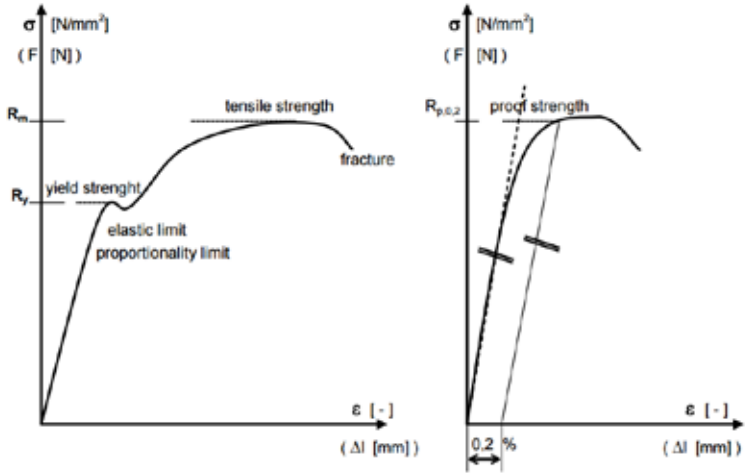

Fig. 9. Definition of relevant mechanical properties examined for each batch of material

References

[1] Green J.A.S. *Aluminum recycling and processing for energy conservation and sustainability*. Materials Park, OH: ASM International, 2007.

[2] Liu Z-K. *Effect of impurities on alloys*. I.T. Program. Washington, DC: Energy Efficiency and Renewable Energy, US Department of Energy, 2003.

[3] Gesing A. *Journal of Materials.* 2004, 56, 18–27.

[4] Kim J-Y., Kim S-J., Song I-K., Han J-H. *Aging characteristics of recycled ACSR wires for distribution lines.* Electrical insulation conference and electrical manufacturing & coil winding conference, 1997.

[5] Viklund-White C. and Menad N. *Impurity accumulation as a consequence of increased scrap recycling.* Stockholm, Sweden: Minerals and Metals Recycling Research Centre, MiMeR Lulea University of Technology, 1999, pp. 35.

[6] Lundqvist U., Andersson B., Axsater M., Forsberg P., Heikkila K. and Jonson U. et al. *Design for recycling in the transport sector – future scenarios and challenges.* Goteborg, Sweden: Chalmers University of Technology, Goteberg University, 2004.

[7] Das S.K. *Light Metals*, TMS, 2006, 911-916.

[8] Gesing A. and Harbeck H. *Particle sorting of light-metal alloys and expanded use of manufacturing scrap in automotive, marine, and aerospace markets*. In: Global symposium on recycling, waste treatment, and clean technology (REWAS), 2008.

[9] Gaustad G., Olivetti E., Kirchain R. *Journal of Industrial Ecology*, 2010, 14, 286–308.

[10] Phillip H.W.L. *Annotated equilibrium diagrams of some aluminium alloy systems*. London, Institute of Metals, 1959.

[11] Mondolfo L.F. *Aluminium alloys: structure and properties*. London: Boston, Butterworths, 1976.

[12] Kral M.V. A crystallographic identification of intermetallic phases in Al-Si alloys. *Materials Letters*, 2005, 59, 2271-2276.

[13] Phillips H.W.L. and Varley P.S. The constitution of alloys of aluminium with manganese, silicon and iron. III – The ternary system: aluminium-silicon-iron. IV – The quaternary system: aluminiummanganese-silicon-iron. *Journal of the Institute of Metals*, 1943, 69, 317-350.

[14] Phragmén G. On the phases occurring in alloys of aluminium with copper, magnesium, manganese, iron and silicon. *Journal of the Institute of Metals*, 1950, 77, 489-552.

[15] Couture A. Iron in aluminium casting alloys – a literature survey, American Foundryman's *Society. International Cast Metals Journal*, 1981, 6 (4), 9-17.

[16] Crepeau P.N. Effect of iron in Al-Si alloys: a critical review. Transactions of the American *Foundryman's Society*, 1995, 103, 361-366.

[17] Taylor J.A. Metal-related castability effects in aluminium foundry alloys. *Cast Metals*, 1995, 8 (4), 225-252.

[18] Mbuya T.O et al. Influence of iron on castability and properties of aluminium silicon alloys*:* literature review. *International Journal of Cast Metals Research*, 2003, 16 (5), 451-465.